© 2016. Published by The Company of Biologists Ltd | Journal of Cell Science (2016) 129, 2829-2840 doi:10.1242/jcs.179655

RESEARCH ARTICLE

The Rho GTPase Rif signals through IRTKS, Eps8 and WAVE2 to generate dorsal membrane ruffles and filopodia

Thankiah Sudhaharan[1], Kai Ping Sem[1], Hwi Fen Liew[1], Yuan Hong Yu[1], Wah Ing Goh[1,2], Ai Mei Chou[1] and Sohail Ahmed[1,*]

ABSTRACT

Rif induces dorsal filopodia but the signaling pathway responsible for this has not been identified. We show here that Rif interacts with the I-BAR family protein IRTKS (also known as BAIAP2L1) through its I-BAR domain. Rif also interacts with Pinkbar (also known as BAIAP2L2) in N1E-115 mouse neuroblastoma cells. IRTKS and Rif induce dorsal membrane ruffles and filopodia. Dominant-negative Rif inhibits the formation of IRTKS-induced morphological structures, and Rif activity is blocked in IRTKS-knockout (KO) cells. To further define the Rif–IRTKS signaling pathway, we identify Eps8 and WAVE2 (also known as WASF2) as IRTKS interactors. We find that Eps8 regulates the size and number of dorsal filopodia and membrane ruffles downstream of Rif–IRTKS signaling, whereas WAVE2 modulates dorsal membrane ruffling. Furthermore, our data suggests that Tir, a protein essential for enterohemorrhagic *Escherichia coli* infection, might compete for Rif for interaction with the I-BAR domain of IRTKS. Based on this evidence, we propose a model in which Rho family GTPases use the I-BAR proteins, IRSp53 (also known as BAIAP2), IRTKS and Pinkbar, as a central mechanism to modulate cell morphology.

KEY WORDS: IRTKS, Eps8, WAVE2, Dorsal filopodia, Dorsal ruffles

INTRODUCTION

The Rho GTPases Rif (for 'Rho in filopodia') and Cdc42 are known to signal to the actin cytoskeleton (Hall, 2012). Both GTPases can generate filopodia, dynamic structures that are thought to be involved in cell sensing mechanisms. Cdc42 partners with the Inverse bin-amphiphysin-Rvs (I-BAR) protein IRSp53 (insulin receptor substrate protein 53 kDa; also known as BAIAP2) in inducing filopodia formation (for a review, see Scita et al., 2008). IRSp53 has a Cdc42-binding site and an SH3 domain, both of which are crucial for filopodia formation (Krugmann et al., 2001; Govind et al., 2001). The IRSp53 SH3 domain interacts with Mena (also known as ENAH) (Krugmann et al., 2001), Eps8 (Disanza et al., 2006), WAVE2 (also known as WASF2) (Suetsugu et al., 2006; Goh et al., 2012), mDia1 (Goh et al., 2011) and dynamin 1 (Chou et al., 2014) to induce filopodia. These data led to a model for filopodia formation mediated by IRSp53 where membrane protrusion modulated by its I-BAR domain is coupled to actin polymerization modulated by its SH3-domain-binding partners (Ahmed et al., 2010). Cdc42 is thought to activate and localize IRSp53 (Disanza et al., 2006). As for Rif, it has been found to partner the actin nucleators mDia1 and mDia2 in forming peripheral filopodia (Goh et al., 2011; Pellegrin and Mellor, 2005).

The I-BAR family of proteins contain five members: IRSp53, IRTKS (insulin receptor tyrosine kinase substrate; also known as BAIAP2L1 or BAI1-associated protein 2-like 1), MIM (missing in metastasis; also known as MTSS1), ABBA (actin-bundling protein with BAIAP2 homology; also known as MTSS1L), and Pinkbar (Planar intestinal-and kidney-specific BAR domain protein; also known as BAI1-associated protein 2-like protein 2, BAIAP2L2). The I-BAR domain induces membrane tubulation with variation for each family member (Saarikangas et al., 2009; Mattila et al., 2007). I-BAR proteins are thought to dimerize allowing membrane curvature to be induced (Zhao et al., 2011). The domain structure of I-BAR family proteins suggest coupling of I-BAR domain-induced membrane deformation with signaling pathways associated with the actin cytoskeleton (Scita et al., 2008) that could give rise to actin-based cell membrane protrusions. Such protrusions have been shown to play roles in pathological conditions such as infection and metastasis. For example, enteropathogenic and enterohemorrhagic *Escherichia coli* trigger the formation of an actin-based membrane protrusion on the apical surface of host cells known as the actin pedestal. IRSp53 and IRTKS have been implicated in this process. In particular, IRTKS is subverted by the *E. coli* proteins translocated intimin receptor (Tir) and Tir cytoskeleton coupling protein (TccP) (Vingadassalom et al., 2009), and Tir is known to bind the I-BAR domains of IRTKS and IRSp53 (Vingadassalom et al., 2009; Weiss et al., 2009). Invadosomes are another type of actin-based cell membrane protrusion that facilitate the migration of cancer cells (see Linder et al., 2011 for a recent review). Thus, it is important to understand the signaling pathways that lead to the formation of actin-based membrane protrusions at the dorsal surface of cells.

Rif has been shown to induce dorsal protrusions in wide-field (Goh et al., 2011) and confocal imaging (Pellegrin and Mellor, 2005) studies. However, to follow dorsal morphology quantitatively it is important to use a technique such as scanning electron microscopy (SEM). The signaling pathway by which Rif generates dorsal structures, such as dorsal membrane ruffles and filopodia, is unknown. Using affinity purification and mass spectrometry analysis, we identify IRTKS as a Rif interactor. Both IRTKS and Rif induce dorsal filopodia and membrane ruffles. We also identify Eps8 and WAVE2 as modulators of this dorsal morphology downstream of Rif and IRTKS. Thus, we establish a new pathway, Rif to IRTKS to Eps8 and WAVE2, responsible for the generation of dorsal filopodia and membrane ruffles.

RESULTS

To identify Rif targets we used a tandem affinity purification tag approach (Rigaut et al., 1999). A number of proteins that bound

[1]Neural Stem Cell Laboratory, Institute of Medical Biology, 8A Biomedical Grove, Immunos, 138648 Singapore. [2]Mechanobiology Institute, National University of Singapore, 5A Engineering Drive 1, 117411 Singapore.

*Author for correspondence (sohail.ahmed@imb.a-star.edu.sg)

S.A., 0000-0002-5208-8193

Received 25 August 2015; Accepted 27 May 2016

Journal of Cell Science

Journal of Cell Science (2016) 129, 2829-2840 doi:10.1242/jcs.179655

specifically to Rif were identified. In this paper, we analyze one of these Rif-binding proteins – IRTKS. To confirm that Rif does indeed interact with IRTKS we carried out pulldown experiments using HA-tagged proteins. As controls, we used IRSp53 and a constitutively active version of mDia1 (mDia1ΔDAD). Rif interacted with IRTKS and the mDia1ΔDAD, but not with IRSp53 (Fig. 1A). Next, we asked whether other members of the I-BAR family of proteins interacted with Rif. Our results show Rif interacts with Pinkbar in addition to IRTKS but not with MIM, ABBA or IRSp53 (Fig. 1B). To determine the Rho family GTPase specificity of IRTKS we used RhoA, Cdc42 and Rac in pulldown experiments. IRTKS showed high specificity for Rif independently of its GTP- or GDP-bound status (Fig. 1C,D). The location of the Rif-binding site on IRTKS was identified using a series of deletion constructs. Rif bound to the I-BAR domain but not to other regions of IRTKS (Fig. 1E,F).

To analyze the morphological signaling pathway that the Rif–IRTKS complex is involved in, we used the mouse neuroblastoma cell line N1E-115. Expression of IRTKS itself induced filopodia formation, both peripheral and dorsal, as well as dorsal membrane ruffles (Fig. 2A), and this phenotype of IRTKS is similar to that induced by Rif (Ellis and Mellor, 2000; Fan and Mellor, 2012; Goh et al., 2011). When IRTKS was expressed with constitutively active Rif (mutation Q77L), denoted RifL77, there was a synergy, giving an enhanced phenotype (Table 1). In contrast, when IRTKS was expressed with dominant-negative Rif (mutation T33N), denoted RifN33, there was a reduction in the phenotype, as seen by a 50% reduction in filopodia formation.

To confirm that Rif and IRTKS interacted in a cellular context, we carried out fluorescence resonance energy transfer (FRET) experiments using fluorescence lifetime imaging microscopy (FLIM). These FLIM experiments also revealed the location of the Rif–IRTKS interaction within the cell. There was a decrease of GFP–Rif lifetime in the presence of IRTKS ($P<0.003$) yielding a FRET efficiency of 6.3%, indicating that Rif and IRTKS do interact (Fig. 2B). The Rif–IRTKS complex appeared to be located on peripheral and dorsal filopodia and membrane ruffles. To locate the region in Rif responsible for the interaction with IRTKS, we generated RifS51A, RifE54N and RifΔCAAX deletion mutations and examined localization and interaction using confocal imaging and FLIM-FRET measurement, respectively. Initially, we carried out confocal imaging by co-expressing GFP–IRTKS with mCherry–Rif or its mutants. The confocal data (Fig. S1A) suggests that there is distinct localization of Rif mutants in N1E 115 cells. RifE51A and RifE54N colocalized with IRTKS along the edges of cells whereas the RifΔCAAX mutant localized in the nucleus of cells. The FLIM data (Fig. S1B) revealed that the RifS51A had a minimal interaction with IRTKS compared with RifQ77L, followed by RifE54N and RifΔCAAX. These data suggest that the amino acid E54 and the CAAX motif are essential for Rif interaction with IRTKS and generation of dorsal structures.

To further investigate the idea that Rif signals through IRTKS to generate dorsal actin-based structures, we generated IRTKS-knockout (KO) mice (Fig. S1C) and then derived KO mouse embryonic fibroblast (MEF) cell lines from them. IRTKS-KO mice had no obvious phenotype. Rif failed to generate dorsal filopodia and membrane ruffles in IRTKS-KO cells (Fig. 2C), whereas Rif generated intense peripheral edge ruffling (arrowhead, Fig. 2C) and long peripheral protrusions (arrowhead, Fig. 2C) in IRTKS KO cells. On rescue of these KO cells with IRTKS, the Rif–IRTKS dorsal phenotype was restored (Fig. 2C). Given that Rif interacts with Pinkbar (based on pulldown and immunoblot experiments) there was a possibility that the edge ruffling and long protrusions induced by Rif in IRTKS KO cells are due to Pinkbar. Interestingly, we found that Pinkbar located with Rif in edge ruffling sites but not with the long protrusions (Fig. 2C). As controls, we showed that the IRTKS I-BAR domain alone and the IRTKS SH3 domain mutant are not able to rescue the lack of dorsal phenotype in IRTKS KO cells (Fig. 2D).

Table 1. IRTKS induces filopodia in N1E-115 cells

Protein(s) expressed	Filopodia per cell	Filopodial length (μm)	Filopodial lifetime (s)
GFP–actin	1.2±1.02	7.16±0.82	212±64
RifQL+GFP–actin*	8.5±2.36	4.37±0.28	162±14
mCherry–ABP**	1.3±1.03	4.68±1.01	166±17
GFP–IRTKS +mCherry–ABP	10.0±0.22	3.60±0.44	113±8
GFP–IRTKS +mRFP–RifL77	14.3±4.19	ND	ND
GFP–IRTKS +mRFP–RifN33	5.1±2.57	ND	ND

Cells were transfected with GFP–IRTKS and mCherry–Lifeact and imaged using dual-channel (GFP and mCherry) time-lapse microscopy at 24 h post transfection. Filopodia number, length and lifetime were then scored as described previously (Lim et al., 2008). Data is expressed as mean±s.d. (n=3–7). Data from *Goh et al., 2011 and **Goh et al., 2012 is shown for comparison, but excluded from statistical analysis. ND, not detected.

Next we turned to SEM to analyze and quantify dorsal filopodia and membrane ruffles. In control cells expressing GFP or mRuby we did not detect surface protrusions (Fig. 2E). Upon expression of IRTKS or Rif alone, structures resembling small filopodia were seen, designated here as filopodial tips (Fig. 2E; Fig. S1D). With coexpression of IRTKS and Rif, dorsal filopodia and membrane ruffles were clearly seen (Fig. 2E, bottom right panel). In IRTKS KO cells, overexpression of Rif induced only dorsal filopodial tips. Interestingly, Rif also induced edge ruffling and long peripheral protrusions in IRTKS KO cells (Fig. 2E, right panel). In contrast, Rif expression in IRTKS KO cells rescued with IRTKS revealed both dorsal filopodia and membrane ruffles (Fig. 2E, bottom panel). Fig. 2F shows a quantification of the results presented in Fig. 2E. In order to test the role of Rif in a more physiological manner, we carried out 3D imaging of cells in 3D culture in a collagen type I matrix (Fig. S2A; Movies 1 and 2). All cells generated surface protrusions that are not seen in the control experiments. Thus, in both 2D and 3D cultures, Rif induces filopodia and membrane ruffles.

Having established that Rif signals through IRTKS to generate dorsal filopodia and membrane ruffles, we next investigated possible partners of IRTKS that could be involved in this process. Based on the fact that the SH3 domain of IRSp53 plays a crucial role in peripheral filopodia formation through proteins such as Mena, Eps8 and mDia1, we looked for SH3-domain-binding partners of IRTKS. A mitochondrial localization signal was placed on IRTKS–mRuby with the idea that proteins interacting with IRTKS would relocalize to mitochondrial sites (Kanaji et al., 2000). HeLa cells coexpressing mito-IRTKS–mRuby and potential GFP-tagged interacting partners (WAVE1, WAVE2, Mena, Eps8, VASP, Espin, mDia1, mDia2, N-WASP, ezrin, dynamin 1 and dynamin 2) were generated, and colocalization analysis carried out

Journal of Cell Science (2016) 129, 2829-2840 doi:10.1242/jcs.179655

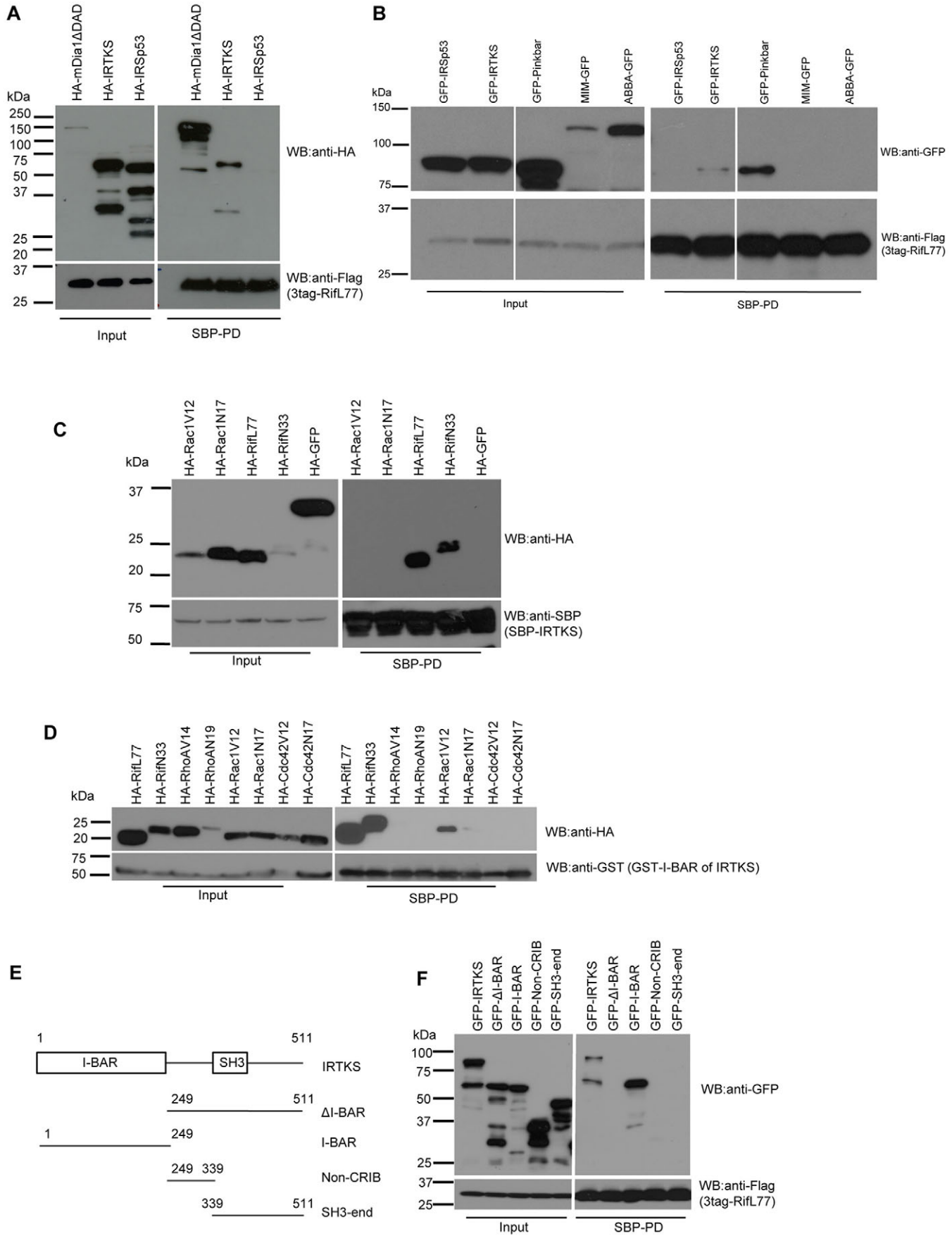

Fig. 1. See next page for legend.

Journal of Cell Science (2016) 129, 2829-2840 doi:10.1242/jcs.179655

Fig. 1. Characterization of Rif interaction with IRTKS. (A) Rif interacts with IRTKS. 3tag–RifL77 was coexpressed with either HA-tagged mDia1ΔDAD, IRTKS or IRSp53 in 293T cells and analyzed for pairwise interactions by SBP pulldown (SPD-PD) of Rif and immunoblotting (WB) with anti-HA antibody. Rif was detected using anti-Flag antibody as described in the Materials and Methods section. (B) Rif interacts with Pinkbar. 3tag–RifL77 was coexpressed with either GFP-tagged IRSp53, IRTKS, Pinkbar, MIM or ABBA in 293T cells and analyzed for pairwise interactions by SBP pulldown of Rif and immunoblotting with anti-GFP antibody. Rif was detected using anti-Flag antibody. (C,D) Rif interacts with IRTKS specifically. (C) SBP fusion of full-length IRTKS was coexpressed with HA-tagged constitutively active (Rac1V12, RifL77) or dominant-negative versions (RacL77, RifN33), respectively, of Rac1 and Rif, or GFP in 293T cells, and pairwise interactions were analyzed by SBP pulldown of IRTKS and immunoblotting with anti-HA antibody. IRTKS was detected using anti-SBP antibody. (D) A GST fusion of the I-BAR domain of IRTKS was coexpressed with HA-tagged constitutively active or dominant-negative versions, respectively, of Rif (L77, N33), RhoA (V14, N19), Rac1 (V12, N17) and Cdc42 (V12, N17) in 293T cells and analyzed for pairwise interactions by GST pulldown of Rif and immunoblotting with anti-HA antibody. The I-BAR domain of IRTKS was detected using anti-GST antibody. (E) A schematic of the domain structure of full-length human IRTKS protein and deletion constructs with their abbreviations shown. Numbering is based on amino acids. (F) Localization of Rif interaction site on IRTKS. 3tag–RifL77 was expressed with either GFP-tagged IRTKS full-length or deletions named ΔI-BAR, I-BAR, Non-CRIB or SH3-end in 293T cells and analyzed for pairwise interactions by SBP pulldown of Rif and immunoblotting with anti-GFP antibody. Rif was detected using anti-Flag antibody. Transfection, pulldown and immunoblotting were performed as described in the Materials and Methods section.

(Fig. S2B). Positive interactors were defined as candidates with Pearson coefficient values greater than 0.7. Two of the IRTKS interactors identified by this assay were Eps8 and WAVE2 (Fig. 3A). To provide further evidence that Eps8 is indeed an interacting partner of IRTKS, we carried out pulldown and FRET experiments (Fig. 3B,C). IRTKS was able to pull down Eps8 and had a FRET efficiency of 13.48% as measured by FLIM, thus providing strong evidence for the interaction ($P<0.0001$). Further, using deletion mutants of Eps8 and FRET-based assays, we were able to localize IRTKS binding to the C-terminal of Eps8 (amino acids 648–821; Fig. S3A,B) which is the same region that has been shown to bind IRSp53 (Disanza et al., 2006).

Next, we used SEM analysis to evaluate the role of Eps8 in Rif–IRTKS-induced structures by using Eps8-KO cells (Fig. S3C). Rif and IRTKS were expressed independently in Eps8-KO cells or in Eps8-KO cells reconstituted with Eps8. Rif and IRTKS were able to induce filopodia in the absence of Eps8, suggesting that Eps8 is not essential for this activity (Fig. 3D). The main effect of Eps8 on dorsal filopodia was to reduce their size, converting 'long filopodia' to filopodia (Fig. 3D–F). To quantify the dorsal membrane ruffling activity, we counted the number and length of these structures. Total length was derived from the product of the number and length values. Similar to the effect shown on filopodia, the effect of Eps8 was to reduce the length of dorsal membrane ruffles (Fig. 3F). Another effect of Rif in Eps8-reconstituted cells was an increase in the number of these structures. Thus, Eps8 might also play a role in the generation of dorsal membrane ruffles (Fig. 3F).

We found WAVE2 to be a potential interacting partner of IRTKS in the mitochondrial relocalization assay (Fig. 3A). To further explore this, we examined the location of endogenous proteins in cells expressing Rif and IRTKS. We found that COS-7 cells produced the strongest phenotype of intense dorsal ruffling, when Rif and IRTKS were expressed together (as observed by live cell imaging; Fig. 4A). Based on this, we tried to determine whether we could detect colocalization of IRTKS with the endogenous actin regulatory proteins within dorsal membrane ruffles (Fig. S4A). The antibody specificity of WAVE1 is shown in Fig. S4B (for that of WAVE2, see Goh et al., 2011). Based on the results of Pearson colocalization analysis, WAVE2 but not WAVE1 was found to colocalize with IRTKS at sites of intense dorsal membrane ruffling (Fig. 4B). To confirm that IRTKS could interact with WAVE2, we carried out FRET experiments using FLIM and found these two proteins had a FRET efficiency of 16.3%. Fig. 4C shows that IRTKS indeed interacted with WAVE2 ($P<0.01$) at the sites of dorsal membrane ruffling. Interestingly, we also observed IRTKS colocalization with IRSp53 or Pinkbar (Fig. 4B). Similar to in HeLa cells, Eps8–IRTKS colocalization was also observed in COS-7 cells. Pinkbar is expressed in the control MEF cell line but not in IRTKS-KO cells (see RT-PCR data; Fig. S4C).

To determine whether WAVE2 was required for dorsal membrane ruffling we carried out knockdown (KD) experiments using Dicer substrate small interfering RNAs (DsiRNAs; see Materials and Methods for detail). Again we measured dorsal membrane ruffling activity by scoring for the number and length of such structures. SEM analysis was used to quantify the effect of WAVE2 KD on dorsal membrane ruffling (Fig. S4D). Fig. 4D,E shows that WAVE2 KD reduced the number and length of the dorsal membrane, resulting in a reduction of such morphological activity by 61%. To support the SEM analysis, we also carried out WAVE2 KD and rescue and scored the phenotype based on confocal images of membrane ruffles (Fig. 4F,G). WAVE2 KD resulted in a 54% reduction in membrane ruffling activity (Fig. 4G).

DISCUSSION

Here, we show that Rif interacts with IRTKS through its I-BAR domain. The I-BAR domain of IRTKS has been shown to interact with Tir, an *E. coli* protein involved in actin pedestal formation (Vingadassalom et al., 2009). We found Rif to interact with the I-BAR domain of IRTKS, which is also known to interact with Tir, suggesting that by displacing Rif from IRTKS, Tir could facilitate *E. coli* infection by subverting the physiological pathway responsible for dorsal filopodia and membrane ruffle formation.

We found that Rif interacted with IRTKS and Pinkbar but not the I-BAR proteins IRSp53, MIM and ABBA. Pinkbar has been linked with edge ruffling at cell–cell contacts (Pykalainen et al., 2011). We found that Rif and Pinkbar colocalize and induce edge ruffling. Thus, Rif might play a role with Pinkbar in driving other dorsal cell morphologies. IRTKS did not interact with Cdc42, RhoA or Rac, making it a specific target for Rif. IRTKS bound to both constitutively active and dominant-negative forms of Rif, suggesting no preference for its activation state. MIM and ABBA do not have Rho-GTPase-binding sites, but they might connect to RhoGTPase signaling indirectly through I-BAR family heterodimer formation (see below and Fig. 5).

We have identified Eps8 and WAVE2 as two actin regulators involved in the Rif–IRTKS pathway to dorsal structures. By FRET analysis we show that both Eps8 and WAVE2 bind IRTKS in these dorsal structures. Using SEM we were able to quantify the number and size of dorsal structures generated by the Rif–IRTKS pathway. We found that Eps8 was not essential for dorsal filopodia formation but is involved in modulating their size. This is consistent with the actin-capping role of Eps8 (Croce et al., 2004), where Eps8 prevents the actin filament elongation. In contrast, WAVE2 KD dramatically reduced the number of dorsal membrane ruffles formed and their

Journal of Cell Science (2016) 129, 2829-2840 doi:10.1242/jcs.179655

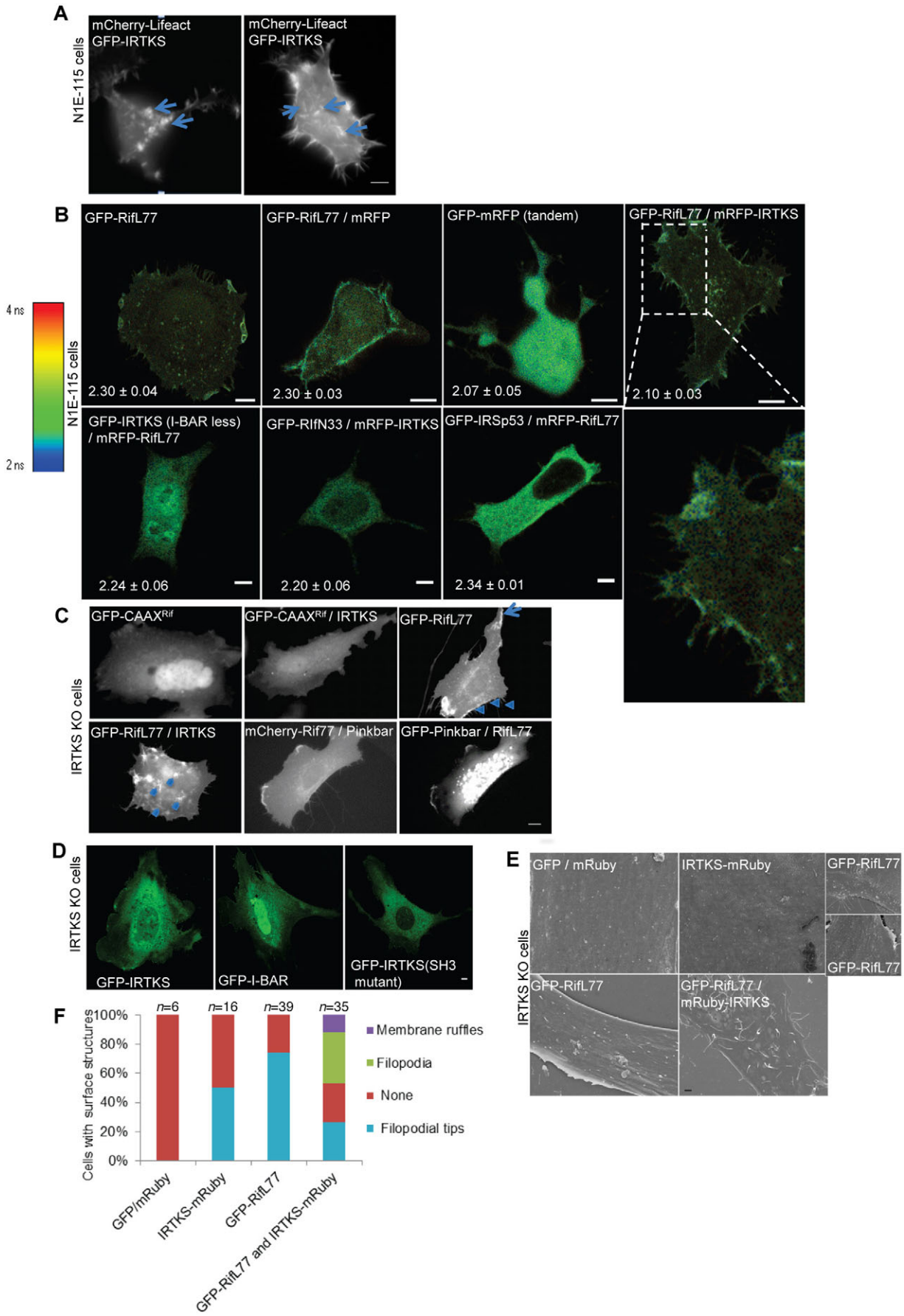

Fig. 2. See next page for legend.

Journal of Cell Science

Journal of Cell Science (2016) 129, 2829-2840 doi:10.1242/jcs.179655

Fig. 2. Rif signals through IRTKS to generate dorsal morphology. (A). IRTKS phenotype in N1E-115 cells. Cells were transfected with GFP–IRTKS and mCherry–Lifeact. Dual-channel (GFP and mCherry) time-lapse microscopy was then carried out at 24 h post transfection as described in the Materials and Methods section. Two typical cells are shown. Left panel: dorsal membrane ruffles (arrows). Right panel: dorsal filopodia (arrows). Scale bar, 10 µm. (B) Rif interacts with IRTKS as observed by FLIM-FRET. Representative FLIM images of N1E115 cells expressing (top panels, left to right): GFP–RifL77, coexpression of GFP–RifL77 and mRFP, GFP–mRFP (tandem), and coexpression of GFP–RifL77 and mRFP–IRTKS; (bottom panels, left to right): coexpression of GFP–IRTKS (lacking the I-BAR domain, I-BAR less) and mRFP–RifL77, GFP–RifN33 and mRFP–IRTKS, GFP–IRSp53 and mRFP–RifL77 (negative control), and magnified image of top panel GFP–RifL77 and mRFP–IRTKS. Numbers on images represent the respective lifetimes in ns. Scale bars: 5 µm. Data is expressed as mean±s.d. (n=5–7 cells). (C). Rif requires IRTKS for generation of dorsal structures. Cells were imaged using dual-channel live-cell microscopy. IRTKS-KO MEFs were isolated from KO mice and transfected with the relevant cDNAs. Representative examples are shown of individual cells expressing (top panels, left to right) GFP–$CAAX^{Rif}$ (plasma membrane localization motif CAAX from the C-terminal end of Rif), GFP-$CAAX^{Rif}$ and IRTKS, and GFP–RifL77; and (bottom panel, left to right) coexpression of GFP–RifL77 and IRTKS, coexpression of mCherry–RifL77 and Pinkbar, and coexpression of RifL77 and GFP–Pinkbar. Membrane ruffles (arrow) and peripheral protrusions (arrowheads) are found in the GFP–RifL77 cells, whereas dorsal protrusions (arrowhead) are seen upon coexpression of GFP–RifL77 and IRTKS. Scale bar: 10 µm. (D) Rescue of IRTKS-KO cells upon expression of GFP–IRTKS, GFP–I-BAR or GFP–IRTKS (SH3 mutant). Scale bar: 5 µm. (E) Rif requires IRTKS for generation of dorsal structures. IRTKS-KO MEFs isolated from KO mice were transfected with the relevant cDNAs and grown on gridded coverslips. Cells were then localized by fluorescence imaging and the same cell imaged by SEM. Representative examples are shown of cells expressing GFP and mRuby, IRTKS–mRuby, GFP–RifL77 and upon coexpression of GFP–RifL77 and mRuby–IRTKS. Scale bar: 1 µm. (F) Statistical analysis of data shown in E. Cells were scored for dorsal membrane ruffles, dorsal filopodia and filopodial tips as described in the Materials and Methods. The images of individual cells shown are representative of cells when searching for dorsal protrusions.

length. Eps8 also reduced the size of dorsal membrane ruffles, but increased their number.

Invadosomes have been linked to cell migration and cell invasion connected with small GTPases (Spuul et al., 2014). The actin machinery responsible for the formation of invadosomes includes actin modulators such as fascin and small GTPases. Is it possible that actin pedestals and invadosomes subvert the machinery used to generate dorsal filopodia and membrane ruffles? If this is the case one would predict that Rif, IRTKS and downstream targets such as Eps8 and WAVE2 are involved in the formation of these disease-related dorsal structures. Interestingly, we have observed endogenous Eps8 in the actin pedestals triggered by enterohemorrhagic *E. coli* infection of SKOV3 ovarian cancer cells (A.M.C. and S.A., unpublished data).

Rac and Cdc42 have been shown to generate peripheral structures (membrane ruffles and filopodia, respectively) through IRSp53. Here, we show using an SEM assay that Rif, in contrast to Rac and Cdc42, modulates dorsal membrane ruffles and filopodia. Rif requires IRTKS to generate these dorsal structures and also utilizes Pinkbar. In Fig. 5 we present a model showing the interrelationships between these pathways. In preliminary experiments, we observed with FRET the formation of heterodimers of I-BAR domain proteins, which would suggest cross-talk between Rac, Cdc42 and Rif, and the possibility to generate diverse morphological structures. Further work is necessary to determine the physiological consequences of heterodimer formation. Nevertheless, the ability of I-BAR domain proteins to heterodimerize highlights two important issues – the diversity of morphological structures generated by and the complexity of Rho GTPase signaling. In future experiments it will be important to identify growth factors that lead to Rif activation and dorsal morphological activities.

In conclusion, we show that the Rif–IRTKS–Eps8–WAVE2 pathway leads to formation of the dorsal membrane ruffles and filopodia, and suggest that Rac, Cdc42 and Rif utilize I-BAR domain proteins as a central mechanism to regulate cell morphology.

MATERIALS AND METHODS

Plasmid constructs

The pXJ40 mammalian expression vectors with various N-terminal fusion tags used in this study are HA, GFP, GST and mCherry (Manser et al., 1997). The pXJ3tag vector used for tandem affinity purification or pulldown was made as described in Goh and Manser (2010). Briefly, tandem affinity purification makes use of the CBP and SBP tag present in the triple-epitope-tagged (3tag) construct of Rif. The RifL77 mutant was cloned into pXJ3tag using HindIII and NotI sites by PCR from Rif templates (wild-type, Rif with the activating mutation Q77L, and Rif with the dominant-negative mutation T33N; provided by Harry Mellor, Bristol University, Bristol, UK). RifL77 was then excised and inserted into pXJ-HA and pXJ-mCherry. RifN33 was cloned into pXJ-HA using a similar approach. GFP was subcloned into pXJ3tag using BamHI/NotI. pXJ-HA-IRTKS and pXJ-Lifeact-GFP were from Edward Manser (IMCB, Singapore), pXJ-HA-IRTKS-eGFP was created by insertion of IRTKS–EGFP (Pekka Lappalainen, Institute of Biotechnology, Finland) into pXJ-HA vector. pXJ-mCherry-Lifeact was obtained by appending the Lifeact sequence 3′ of mCherry. The C-terminal end of Rif containing the plasma-membrane-targeting motif of CAAX was cloned as a HindIII–NotI fragment into pXJ-GFP for the generation of the CAAX plasmid. GFP–IRTKS (lacking the I-BAR domain) and GFP–IRTKS (SH3 mutant) are in the pXJ-GFP vector. Rif mutations of S51A, E54N and deletion of the CAAX bases were generated in the RifWT-mCherry vector.

The mitochondrial outer membrane targeting vector (pXJ-mito) was made by subcloning the sequence encoding the N-terminal 33 amino acid residues containing the transmembrane domain (TMD) of Tom20 (Addgene 37316) into the pXJ40 vector using EcoRI/BamHI. The TMD fusion will therefore be anchored to the outer membrane of the mitochondria by the TMD, leaving the adjoining fusion protein exposed to the cytosol (Kanaji et al., 2000). pXJ-mito-IRTKS-mRuby was created by inserting mRuby-tagged IRTKS into this pXJ-mito vector. mCherry-C1-Eps8 (Addgene 29779), mtagBFP2 (Addgene 34633), mRuby2 (Addgene 40260), Ezrin-eGFP (Addgene 20680) vectors were obtained from Addgene.

Full-length and truncations of human IRTKS were introduced into pXJ-GFP by BamHI/XhoI with the exception of I-BAR, which was excised using XhoI/BamHI from the I-BAR domain of mouse IRTKS in pEGFP-N1 (Pekka Lappalainen) and ligated into the XhoI/BglII sites of pXJ-GFP. pXJ-GST MIM and ABBA in pEGFP-N1 vector were from Pekka Lappalainen. GFP–Mena vector was a gift from Klemens Rottner (University of Bonn, Germany). EGFP–Eps8, EGFP–Eps8 deletion mutants, EGFP–WAVE1, EGFP–WAVE2, and EGFP–VASP pCDNA3.1 vectors and vectors for Flag-tagged Eps8, Eps8L1, Eps8L2 and Eps8L3 were a gift from Giorgio Scita (IFOM-IEO Campus, Italy). EGFP–Espin vector was a gift from James R. Bartles (Northwestern University, Chicago, IL). pEGFP-N1-human Dyn1(aa) was a gift from Pietro De Camilli (Yale University, New Haven, CT). pEGFP-N1-rat Dyn2(aa) was a gift from Mark A. McNiven (Mayo Clinic, Rochester, MN). GFP–N-WASP vector was a gift from Sylvie Lommel (Department of Cell Biology, German Research Centre for Biotechnology, Braunschweig, Germany). pXJGFPmDia1ΔDAD was made by subcloning from a source of mDia1ΔDAD sequence (ChengGee Koh, NTU, Singapore). pcDNAmyc-GFP-mDia2ΔDAD and pcDNAmyc-HA-mDia2ΔDAD were made by inserting GFP or HA into pcDNAmyc-mDia2ΔDAD (gift from Arthur Alberts, Van Andel Research Institute, Grand Rapids, MI), respectively. GFP-C1-IRSp53 vector was a gift from Mari Masuda (NCCRI, Tokyo, Japan). Mouse WAVE2 (GenBank BC156285) and human Pinkbar (GenBank BC015619) templates were purchased from the PlasmID repository at Harvard Medical School and cloned into pEGFP-C1 and pXJ-EGFP, respectively.

Journal of Cell Science (2016) 129, 2829-2840 doi:10.1242/jcs.179655

A

Protein	PC
WAVE2	0.93
WAVE1	0.55
Mena	0.96
Eps8	0.93
VASP	0.96
Espin	0.78
mDia1	0.80
mDia2	0.51
N-WASP	0.59
Ezrin	0.41
Dyn1	0.49
Dyn2	0.49

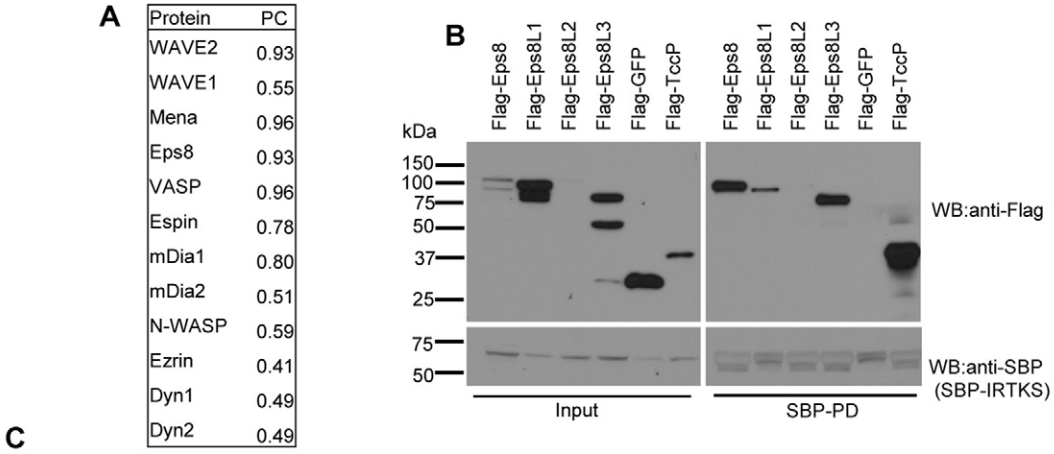

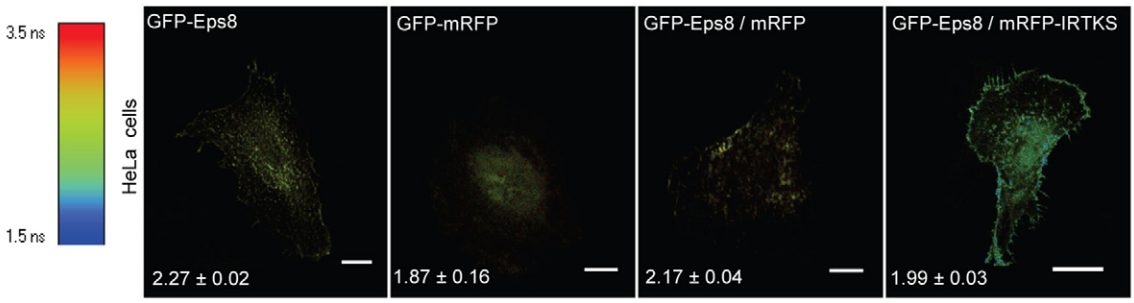

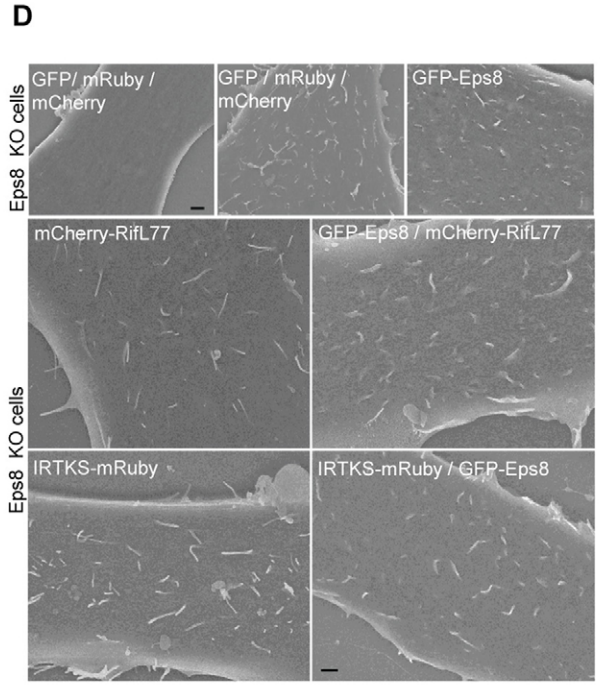

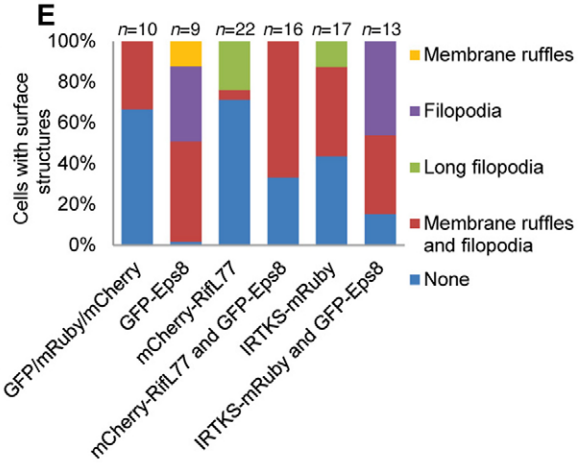

F

Protein(s) expressed	Mean count/cell	Mean length (μm)	Total length (μm)
GFP / mCherry / mRuby	42 ± 4.0	0.80 ± 0.41	30.13 ± 19.25
GFP-Eps8 (reconstitution)	23 ± 9.0	0.60 ± 0.25 *	13.34 ± 06.08
mCherry-RifL77	57 ± 15	1.12 ± 0.49	61.84 ± 29.89
GFP-Eps8 and mCherry-RifL77	88 ± 12	0.72 ± 0.41 *	63.04 ± 36.09
IRTKS-mRuby	51 ± 20	1.45 ± 0.73	71.55 ± 38.53
GFP-Eps8 and IRTKS-mRuby	52 ± 90	0.76 ± 0.37 *	38.89 ± 19.76

Fig. 3. See next page for legend.

Journal of Cell Science

Fig. 3. Eps8 interacts with IRTKS and is involved in the generation of dorsal morphology. (A) Identification of IRTKS partners using mitochondrial localization. Mitochondria-targeted IRTKS–mRuby was coexpressed with GFP-tagged WAVE1, WAVE2, Mena, Eps8, VASP, Espin, mDia1, mDia2, N-WASP, Ezrin, Dyn1 or Dyn2 in HeLa cells. Dual-channel fluorescence live-cell imaging was then carried out. Regions of interest (ROIs) were drawn and Pearson's colocalization coefficients (PC) were calculated using Metamorph software. Pearson's colocalization values above 0.7 were taken as indicative of colocalization (images shown in Fig. S2B). (B) IRTKS interacts with Eps8. SBP–IRTKS was coexpressed with Flag-tagged Eps8, Eps8L1, Eps8L2, Eps8L3, GFP or TccP in 293T cells and pairwise interactions analyzed by SBP pulldown of IRTKS and immunoblotting (WB) with anti-Flag antibody. Note that Eps8L2 gave variable expression in 293T cells and in some experiments could not be seen. Hence we were not able to ascertain its ability to co-immunoprecipitate with IRTKS. L1, L2 and L3 are related independent genes of Eps8. IRTKS was detected using anti-SBP antibody. The strong ECL signal obtained when detecting SBP–IRTKS using HRP-conjugated anti-SBP antibody results in signal bleaching on X-ray films that gives the appearance of multiple bands (bottom right panel). (C) IRTKS interacts with Eps8 by FLIM-FRET. Representative FLIM images of HeLa cells expressing GFP–Eps8, GFP–mRFP, coexpression of GFP–Eps8 and mRFP, and GFP–Eps8 and mRFP–IRTKS. Numbers on images represent the respective lifetimes in ns. Scale bars: 10 µm. Data is expressed as mean±s.d. (n=5–7 cells). (D) Effect of Eps8 KO on Rif–IRTKS induction of dorsal morphology as shown by SEM. A GFP, mRuby and mCherry control is shown in the top left and top middle panels, a GFP–Eps8 rescue is shown in the top right panel, mCherry–RifL77 and IRTKS–mRuby are shown in the middle left and bottom left panels, and mCherry–RifL77 and IRTKS–mRuby with Eps8 rescue are shown in the middle left and bottom left panels. Scale bar: 1 µm. (E) Statistical analysis of data shown in D, cells were scored for dorsal membrane ruffles, dorsal filopodia and long dorsal filopodia as described in the Materials and Methods. (F) The mean count, mean length and total length of dorsal membrane ruffling per cell was determined, and expressed as mean±s.d. (n=3–4 cells). Images shown in D were used to assess the size of dorsal membrane ruffles. To score for dorsal membrane ruffling, manual tracing was performed. *P<0.001 (two-tailed t-test).

The primary antibodies

Mouse monoclonal anti-Eps8 (1:100 immunofluorescence, 610143) was from BD Transduction Laboratories; HRP-conjugated mouse monoclonal anti-GAPDH (1:1000 western blotting, G9295), rabbit polyclonal anti-IRSp53 (1:50 IF, HPA023310) and mouse monoclonal anti-Flag (1:7000 western blotting, F3165) were from Sigma-Aldrich; anti-SBP (1:7000 western blotting, sc101595), anti-HA (1:7000 western blotting, sc7392), anti-GFP (1:7000 immunofluorescence, sc9996) anti-Pinkbar (1:50 immunofluorescence, sc86305) anti-GST (1:7000 western blotting, sc-138) and anti-WAVE1 [1:200, goat polyclonal (sc10388) and anti-WAVE2 (1:50 immunofluorescence, sc-33548)] were from Santa Cruz Biotechnology.

Cell culture and transfection

HEK293 (CRL-1573), HEK293T (CRL-3216), COS-7 (CRL1651) cells were from ATCC. N1E-115 neuroblastoma, HeLa and NIH3T3 cells were cultured in Dulbecco's modified Eagle's medium (DMEM; 4500 mg/l glucose) and supplemented with 10% fetal bovine serum and 1% penicillin-streptomycin in a humidified 37°C incubator with 5% CO_2. Cell culture mycoplasma contamination was carried out using PCR for all cells. For N1E-115 cells transient expression of plasmids were performed using Lipofectamine 2000 (Invitrogen) or Jetprime (Polyplus-transfection) according to the manufacturer's instructions. HeLa and NIH3T3 cells transient transfections were performed according to the manufacturer's protocol using TurboFect (Thermo Scientific).

To obtain IRTKS$^{del/del}$ (null) mice, a targeting vector was generated using BAC clones from the C57BL/6J RPCIB-731 BAC library, in which exon 2 of IRTKS was flanked by loxP sites (Taconic). Deletion of exon 2 resulted in loss of function of the BAIAP2L1 gene by generating a frameshift from exon 1 to exons 3 and 4 (premature stop codon in exon 3). The vector was integrated into the TaconicArtemis C57BL/6NTac embryonic stem cell (ESC) line by homologous recombination. Targeted C57BL/6NTac ESCs were microinjected into blastocysts, which were then transferred to pseudo pregnant females. Highly chimeric mice were bred to Flp-Deleter females (strain C57BL/6). Germline transmission was identified by the presence of black, strain C57BL/6, offspring (G1) (Taconic). IRTKS$^{del/del}$ mice were obtained by mating B6-Baiap2l1 conditional KO mice with B6.129P2-ROSA-Cre Ki/Ki mice (gift from Colin Stewart, IMB Singapore), and verified by genotyping PCR. IRTKS-null (KO) fibroblasts were verified by immunocytochemistry. Immortalized IRTKS-null MEFs were derived from IRTKS-null embryos and repeatedly subcultured till bypass of senescence. Immortalized Eps8-null MEFs (Giorgio Scita) were originally derived from Eps8-null E13 embryo and immortalized with the NIH3T3 protocol. These cells had been infected with the empty pBABE Hygro vector and selected with hygromycin (200 µg/ml). All cells were maintained in DMEM (4500 mg/l glucose, 10% FBS and 4 mM L-glutamine) by incubating at 37°C with 5% CO_2. Cells were either transfected with TurboFect (Thermo Scientific) or Jetprime (Polyplus) following the manufacturer's protocols. The animal treatment was performed in accordance with IACUC and NACLAR guidelines and approved by Biological Resource Center, Singapore.

Immunofluorescence and microscopy

Cells grown on glass coverslips were fixed with 4% paraformaldehyde in PBS for 10 min and washed with PBS. Cells were then permeabilized with 0.2% Triton X-100 in PBS for 5 min, washed with PBS and blocked in 5% BSA in PBS for 30 min. Primary antibody diluted in 5% BSA in PBS was then incubated with cells overnight at 4°C, followed by washing with PBS. Cells were next incubated with species-specific Alexa-Fluor-conjugated secondary antibody diluted in 5% BSA in PBS for 45 min, washed with PBS and mounted onto glass slides with Hydromount (National Diagnostics). Live-cell microscopy was performed on an Olympus IX83 live-cell inverted microscope (Olympus, Singapore), equipped with a CoolSNAP CCD HQ2 camera (Roper Photometrics) and on- stage incubation system (Tokai Hit). For live-cell imaging, transfected cells grown on 35 mm ibiTreat optical-quality plastic cell culture dishes (Ibidi) were imaged with a 60×/1.2 NA objective. For time-lapse microscopy, images were acquired at 10 s intervals over a 10-min time period in the appropriate fluorescence channels using MetaMorph software (Molecular Devices).

Tandem affinity purification

Each 15-cm dish of HEK293 cells was transfected with 4 µg of target plasmid and 6 µg of pBluescript carrier, with a total of two dishes per target [3tag–RifL77 and negative control (3tag–GFP)]. At 24 h post transfection, cells were rinsed with PBS and frozen. Cell lysate was prepared by adding lysis buffer (20 mM Tris-HCl, pH 8, 130 mM NaCl, 1% Nonidet P-40, 5 mM $MgCl_2$, 1 mM PMSF, 1× protease inhibitor, 4 mM DTT), frozen and thawed twice, and rocked for 20 min at 4°C for extraction, after which insoluble material was removed by centrifugation. Lysate was then precleared by exposure to glutathione–Sepharose beads for 1 h before removal of beads by pulse spin. The final eluate was obtained following the Interplay mammalian TAP system protocol (Agilent Technologies) and reduced in volume by using a combination of molecular mass cut-off columns (3000 MWCO PES VIVASPIN 500, Sartorius) and speed vacuum. This concentrated sample was mixed with Laemmli sample buffer and DTT to a final concentration of 10 mM, reduced at 60°C for 10 min and S-alkylated with 20 mM idoacetamide at room temperature for 30 min. The treated sample was resolved on a 12% SDS-polyacrylamide gel to about 5–10 mm into the resolving gel. The gel was stained with colloidal Coomassie Blue (BioRad) and destained with water. Further downstream processing by nano-liquid chromatography tandem mass spectrometry (LC-MS/MS) and analysis was carried out by the mass spectroscopy group (Manfred Raida) at the Experimental Therapeutics Centre, Singapore, to generate a preliminary list of protein candidates using the Scaffold software (Proteome Software).

Mass spectrometry analysis

The whole gel lane was cut into three bands of equal sizes and transferred into perforated microtiterplates for in-gel digestion (Proxeon). Tryptic digestion was carried out using 10 ng/ml sequencing grade trypsin (Promega) for 4 h at 37°C in 5 mM triethyl ammonium buffer, pH 8.5. The resulting peptides were eluted with 1% formic acid in water (first step), 60% acetonitrile and 0.1% formic acid (second step), and

Journal of Cell Science (2016) 129, 2829-2840 doi:10.1242/jcs.179655

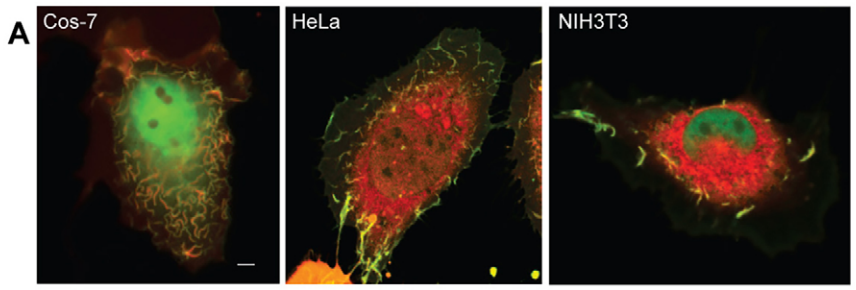

B

Protein	PC
Eps8	0.72
WAVE1	0.36
WAVE2	0.81
IRSp53	0.83
Pinkbar1	0.52
Pinkbar2	0.76

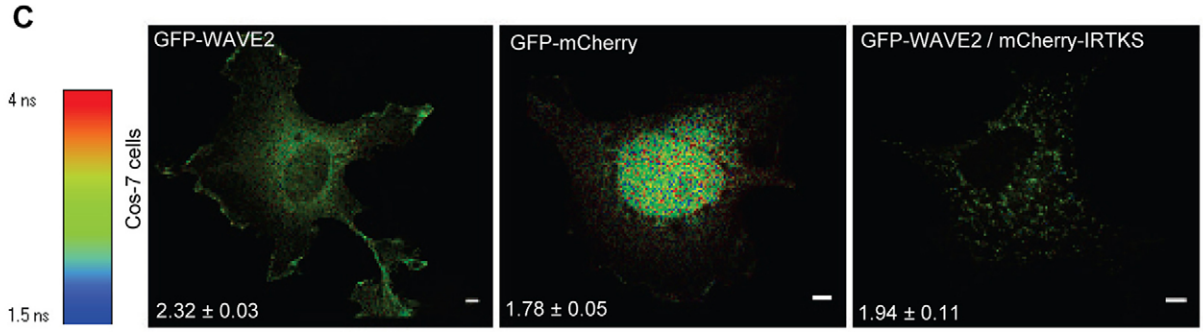

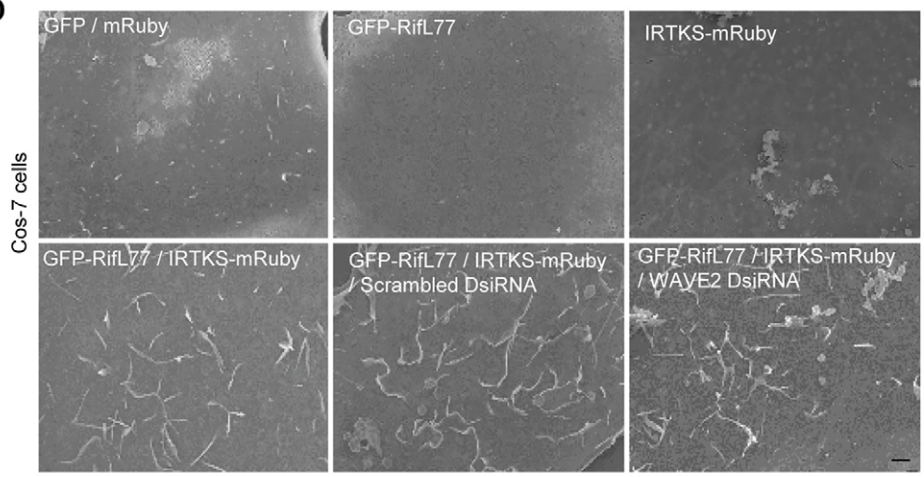

E

GFP-RifL77 and IRTKS-mRuby expressing cells	Mean count/cell		Mean length (μm)		Total length (μm)
Scrambled DsiRNA	35 ± 20	**	4.45 ± 1.48	*	133.74
WAVE2 DsiRNA	20 ± 11		2.23 ± 0.84		52.50

F

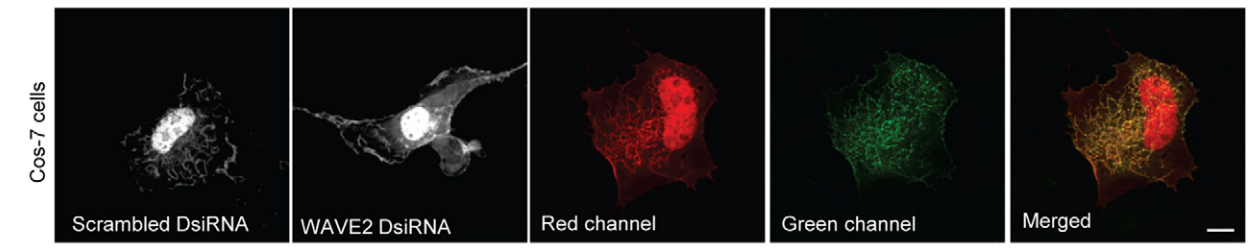

G

n=20	Count			Mean length (μm)			Mean length (μm)			Total length (μm)		
Scrambled DsiRNA	36 ± 15	*		7.5 ± 0.9	***		14.5 ± 3.4	***		271.0 ± 105.0	**	
WAVE2 DsiRNA	24 ± 18		***	6.1 ± 0.7		***	11.0 ± 2.1		***	147.7 ± 117.3		***
Rescue	45 ± 15			9.0 ± 1.1			20.6 ± 5.7			401.1 ± 136.3		

Fig. 4. See next page for legend.

Journal of Cell Science (2016) 129, 2829-2840 doi:10.1242/jcs.179655

Fig. 4. WAVE2 interacts with IRTKS and is involved in the formation of dorsal membrane ruffles. (A) Coexpression of IRTKS and Rif in COS-7, HeLa, and NIH3T3 cells. Cells were transfected with IRTKS–GFP and mCherry–RifL77 as described in the Materials and Methods section and followed by dual-channel live-cell microscopy. Scale bar: 5 µm. (B) IRTKS–GFP colocalizes with endogenous proteins. Endogenous Eps8, WAVE1, WAVE2, IRSp53 and Pinkbar were stained with their respective primary antibodies and Alexa-Fluor-568-conjugated species-specific secondary antibodies. Pearson's colocalization coefficient (PC) values were measured as described in Fig. 3 (images are shown in Fig. S4A). (C) IRTKS interacts with WAVE2 as shown by FLIM-FRET. Representative FLIM images of COS-7 cells expressing GFP–WAVE2, GFP–mCherry (tandem) and both GFP–WAVE2 and mCherry-IRTKS. Numbers on images represents the respective lifetimes in ns. Scale bar: 5 µm. Data is expressed as mean±s.d. (n=5–7 cells). (D) Rif–IRTKS-induced dorsal membrane ruffling is reduced by WAVE2 KD as shown by SEM. Top panels, left to right: GFP and mRuby, GFP–RifL77, and IRTKS-mRuby. Bottom panels, left to right: GFP–RifL77 and IRTKS–mRuby, scrambled DsiRNA with GFP–RifL77 and IRTKS–mRuby, and WAVE2 DsiRNA with GFP–RifL77 and IRTKS–mRuby. Scale bar, 1 µm. (E) Quantification of WAVE2 KD on cell morphology. To score for dorsal membrane ruffling, manual tracing was performed. The mean count, mean length and total length of dorsal membrane ruffling per cell was determined, and expressed as mean±s.d. (n=2–3 cells). *P<0.0001, **P<0.02 (two-tailed t-test). (F) Effect of WAVE2 KD on Rif–IRTKS-induced cell morphology as shown by laser scanning confocal imaging. Representative fluorescence z-stack images of COS-7 cells transfected with mCherry–RifL77 and IRTKS–mRuby and either scrambled DsiRNA (first panel from left), WAVE2 DsiRNA (second panel from left) or rescue with GFP-tagged mouse WAVE2. Representative images of a cell expressing Rif and IRTKS (third panel from left), GFP-tagged mouse WAVE2 (fourth panel from left) and the overlay of the mCherry, mRuby and GFP channels (fifth panel from left). Scale bar: 10 µm. (G) Quantification of the effect of WAVE2 KD on cell morphology. To score for dorsal ruffling, manual tracing was performed plane by plane. The mean, maximum and total length of ruffles per cell were determined, and expressed as mean±s.d. for the n as indicated. *P<0.05, **P<0.01 and ***P<0.001 (two-tailed t-test).

acetonitrile with 0.1% formic acid. The eluted peptides were collected by centrifugation into a new 96-well microtiter plate (Greiner, Germany), frozen at −80°C and freeze dried in a rotary freeze drier. The peptides were then dissolved in 10 ml 0.1% formic acid and submitted to nano-LC-MS/MS analysis. Protein identification was carried out on a QTOF Premier mass spectrometer (Waters), equipped with a Nanospray source. On-line peptide separation was performed on a nanoAcquity UPLC system (Waters) using a 75-mm ID 15-cm column with 1.7 mm C18 material (Waters BEH column). From the sample, 5 ml was injected, trapped on a 300-µm 10-mm trap column and eluted with a gradient from 5% solvent B (0.1% formic acid in acetonitrile) and 95% solvent A (0.1% formic acid in water) to 50% B within 30 min. The overall run time was 60 min at a flow rate of 200 nl/min. Peptides were either identified by data-dependent acquisition (DDA) from the detected peptides with a charge from 2+ to a maximum of 4+, and three precursors were selected for collision-induced fragmentation, or by MSE (Waters) without precursor selection, but switching between low and high energy in the collision cell. The data obtained from the DDA experiments were converted into MGF files using Mascot Distiller (Matrix Science, UK.) and submitted to the MASCOT server (Matrix Science) for database search. The data from the MSE experiments were analyzed with ProteinLynx Global Server 2.3 (Waters). Results from the MASCOT searches were combined using Scaffold (Proteome Software) and filtered for low-score proteins. Proteins identified by one or two peptides were verified manually.

The peptide ADSARTTSTFK was identified after nano-LC-MS/MS using MASCOT Distiller for raw data processing and MASCOT Server for database search against IPI_human. The peptide was identified with a MASCOT ion score of 38.5 and identity score of 44.1, both at the lower border of a sure identification To confirm the result, the MS-TAG search was carried out using the fragment masses which could be clearly identified from the fragment spectrum (y1, y3, y6, y8, y9, y10) and the precursor mass of m/z 592.80. The MS-TAG search was performed on the SWISSPROT database version 2011.01.11 without restriction in the species and an error on precursor and fragments of 100 ppm. The BAIAP2L1 (IRTKS) protein was identified as top hit, no other human proteins where identified by the MS-TAG approach. (http://prospector.ucsf.edu/prospector/cgi bin/msform.cgi?form=mstagstandard)

GST and SBP pulldown

Subconfluent HEK293T cells in 10-cm dishes were transfected with 5 µg each of plasmids encoding bait and prey protein using TurboFect. The following day, confluent cells were scraped into 500 µl of lysis buffer (20 mM HEPES pH 7.3, 100 mM NaCl, 20 mM $MgCl_2$, 1% Triton X-100 and 1 mM DTT) and protease inhibitor cocktail without EDTA (Roche Applied Science) and lysed with rocking at 4°C. After debris removal by centrifugation, cell lysate was mixed with a 50-µl bead volume of streptavidin or glutathione–Sepharose beads (GE Healthcare) and rocked at 4°C for 2 h to allow binding. Beads were repeatedly washed with lysis buffer and eluted using 50 µl of either 2 mM biotin or 20 mM glutathione. For western blot analysis, 10 µl of the lysate (2% input) and 20 µl of the eluate (40% pulldown) were resolved on a 12% SDS-polyacrylamide gel, transferred to a PVDF membranes and immunoblotted with antibodies as specified in the figures and figure legends.

WAVE2 knockdown and rescue

The 27-mer Dicer substrate siRNA to target WAVE2 in COS-7 cells based on the predicted WAVE2 sequence of the African green monkey *Chlorocebus sabaeus*, and the scrambled (negative control). DsiRNAs were designed and synthesized by Integrated DNA Technologies (Singapore). The DsiRNA sequences used are: WAVE2 DsiRNA 5′-GGGCCUGCCUUGUGCUAAACGAUct-3′ and 5′-AGAUCGUUUAGCACAAGGCAGGCCCAC-3′ and WAVE2 negative control DsiRNA 5′CGUUAAUCGCGUAUAAUACGCGUat-3′ and 5′-AUACGCGUAUUAUACGCGAUUAACGAC-3. COS-7 cells seeded onto 18 mm by 18 mm glass coverslips were transfected with DsiRNA at a final concentration of 20 nM using jetPRIME® (Polyplus-transfection SA). The medium was changed at 24 h post transfection. At 32 h post transfection, the DsiRNA-treated cells were then co-transfected with 0.5 µg each of mCherry–RifL77 and HA–IRTKS–mRuby using TurboFect (Thermo Scientific). Cells were fixed and mounted in Vectashield (Vector Laboratories) at 48 h post transfection. As the mouse WAVE2 sequence lacks the targeting sequence of WAVE2 DsiRNA, rescue was mediated by including a small quantity (11 ng) of plasmid DNA encoding EGFP-tagged mouse WAVE2 with the mCherry–Rif77 and HA–IRTKS–mRuby co-transfection mixture and its expression monitored by GFP fluorescence. Although distinguishing the expression of Rif from IRTKS by fluorescence is not possible, dorsal ruffle formation requires the expression of both Rif and IRTKS. Knockdown of WAVE2 was verified by western blotting of lysates prepared from COS-7 cells undergoing various treatments. In order to test specificity of the anti-WAVE1 antibody the WAVE1 siRNA sequence 5′-CGATGAGAAAGGCTTTCCG-3′ and scramble siRNA 5′-CGCTATGAACGGTAGCTGA-3′ were used to reduce the endogenous WAVE1 expression in N1E 115 cells.

RNA extraction and RT-PCR

Total RNA was prepared using Trizol reagent (Thermo Fisher Scientific). Cells were homogenized in 0.8 ml Trizol, and mixed with 0.35 ml chloroform. Samples were then centrifuged at 13,400 ***g*** for 15 min at 4°C. The supernatant was collected and transferred to a spin column (RNeasy Mini Kit, QIAGEN). The subsequent steps leading to RNA isolation were performed according to the manufacturer's protocol. The concentration of RNA was determined using Nanodrop (Thermo Fisher Scientific) and 1 µg of total RNA was reverse transcribed and amplified using the OneStep RT-PCR Kit (QIAGEN). The amplified products were analyzed on 1.5% agarose gels containing ethidium bromide. Primers used were as follows: GAPDH 5′-TGAACCACCAACTGCTTAGC-3′ and 5′-GGCATGGACTGTGGTCATGAG-3′; Pinkbar 5′-AACCGCGTCTTGCTATGGAA-3′ and 5′-TATTCCGAAGACGCTGTGGG-3′.

3D culture

Wild-type MEF cells were transfected with either GFP–CAAX^{Rif} (control) or GFP–RifL77. At 24 h post transfection, cells were trypsinized and

Journal of Cell Science (2016) 129, 2829-2840 doi:10.1242/jcs.179655

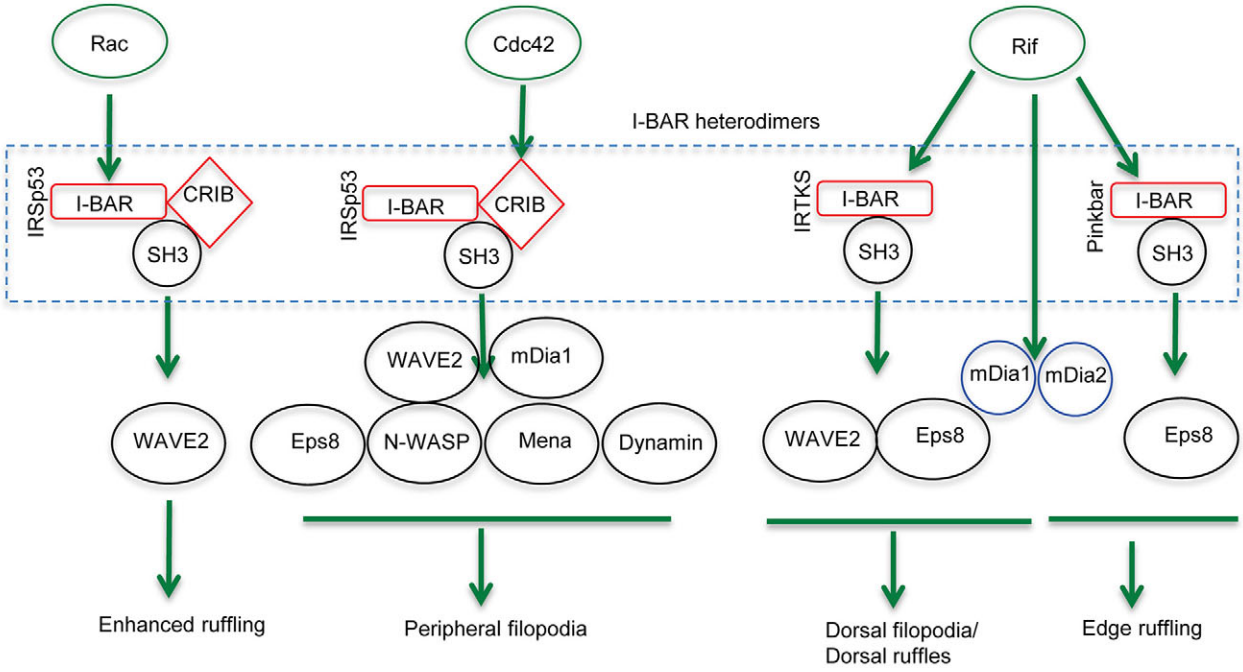

Fig. 5. Rho family GTPases signal through I-BAR proteins to control cell morphology. The data presented in this paper suggests that Rif is responsible for dorsal membrane ruffles and filopodia, whereas Cdc42 and Rac promote peripheral structures. Heterodimerization of I-BAR family proteins allow crosstalk between Rho-family-GTPase-mediated signaling pathways and facilitate the formation of a greater diversity of morphological structures. Although MIM and ABBA do not bind Rac, Cdc42 or Rif, they might be linked to signaling pathways regulated by these Rho family GTPases by forming heterodimers with other I-BAR family proteins. Most importantly, our model suggests that Rif, Rac and Cdc42 utilize I-BAR proteins as a central mechanism for regulating cell morphology.

resuspended in fetal bovine serum at a concentration of 1×10^5 cells/ml. The collagen matrix was prepared and neutralized by mixing 200 µl of type I collagen (Corning) with 250 µl of DMEM medium (Thermo Fisher Scientific) in a pre-cooled 15 ml falcon tube; 23 µl of NaOH (Sigma) was added to collagen to reach neutral pH. Then, 250 µl of cell suspension was then added to the neutralized collagen mixture and plated immediately in a chambered coverglass (Nunc). The collagen mixture was then allowed to solidify completely at 37°C for 3 h. Upon solidification, the gel was overlaid with 200 µl of DMEM and incubated overnight at 37°C. On the following day, 3D imaging was carried out using an inverted confocal microscope.

Fluorescence lifetime microscopy

FLIM experiments were performed on a Time-Correlated Single Photon Counting (TCSPC) system (PicoQuant, Germany) attached to an Olympus FV-1000 confocal microscope (Olympus, USA) with a 60×1.2 W objective (Lam et al., 2012). The excitation light source was a 485-nm pulsed diode laser controlled by a Sepia II driver (PicoQuant) with a 488- or 559-nm dichroic mirror and a 520/30 emission filter. Individual photon arrivals were detected using a SPAD detector and events were recorded by a PicoHarp 300 TCSPC module. Lifetime analysis was carried out using Symphotime software (PicoQuant). Mono- and bi-exponential fittings were obtained for GFP alone and in the presence of mRFP respectively. The percentage FLIM-FRET efficiency was calculated as FRET=100×[1−(lifetime of donor with FRET/lifetime of donor without FRET)].

Scanning electron microscopy

SEM samples were prepared by growing Eps8-KO, IRTKS-KO or COS-7 cells on IBID gridded 35-mm dishes (Zwaenepoel et al., 2012). The cells were transfected with either free GFP or mRuby as controls and fusion plasmids of RifL77, Eps8 and IRTKS alone or in pairs using Turbofect. The WAVE2 KD experiment was performed along with a control experiment in COS-7 cells expressing GFP–RifL77 and IRTKS–mRuby. At 16 h post transfection, cells were fixed using 2.5% glutaraldehyde in 0.1 M sodium cacodylate buffer (pH 7.4) and incubated for at least 20 min at room temperature. Transfected cells were identified under a fluorescence microscope for their locations on the grid and recorded. After fixation, the samples were washed with buffer followed by another 1 h post fixation with 1% osmium tetroxide in 0.1 M sodium cacodylate at 4°C. The samples were extensively washed with distilled water and subsequently dehydrated through a gradient concentration of 25%, 50%, 75%, 95% and 100% ethanol in distilled water. Following two changes of 100% ethanol, the samples were transferred to a Leica Critical Point Dryer (EM CPD 030) for critical point drying to preserve fine cell surface structures. Samples were sputter coated with 2-nm gold and observed using a JEOL Field Emission Scanning Electron Microscope JSM6701F with an accelerating voltage of 5 kV. Cells imaged in fluorescence microscopy were identified in SEM by referring to the marking of the grid.

Colocalization analysis

The degree of colocalization between two proteins at various cell regions was determined by Pearson's coefficient, as previously described (Bu et al., 2009). A value of 0.7 and above was taken as indicating colocalization.

Definition of structures analyzed by SEM

Filopodia tips are defined as small protrusions seen on the dorsal surface. Short filopodia are defined as structures that are smaller than 1 µm, whereas filopodia are defined as structures that are between 1 and 5 µm in length. Dorsal membrane ruffles are defined as sheet-like structures on the dorsal surface of cells (Fig. S1D).

Scoring for dorsal filopodia and membrane ruffling using SEM

The scoring for dorsal filopodia and ruffling was performed using ImageJ software by manual tracing on SEM images for IRTKS-KO, Eps8-KO and COS-7 cells. An average of 2–5 cells of each cell type were scored. The measured lengths were transferred onto an Excel spreadsheet and the mean and total length calculation for filopodia and ruffling was performed.

Statistical analysis

All quantitative results were obtained from at least three independent experiments, and expressed as the mean±s.d. Experimental data were

analyzed by two tailed *t*-test with unequal variance. Differences among samples were considered statistically significant when $P<0.05$.

Acknowledgements
The authors would like to thank John Lim for his help in image analysis and Shuping Lin help in for colocalization analysis.

Competing interests
The authors declare no competing or financial interests.

Author contributions
T.S. and S.A. conceived and designed the experiments and wrote the manuscript. T.S., K.P.S., Y.H.Y., W.I.G. and A.M.C. performed the experiments.

Funding
This work was funded by the Agency for Science, Technology and Research (A-STAR), Singapore.

Supplementary information
Supplementary information available online at
http://jcs.biologists.org/lookup/doi/10.1242/jcs.179655.supplemental

References

Ahmed, S., Goh, W. I. and Bu, W. (2010). I-BAR domains, IRSp53 and filopodium formation. *Semin. Cell Dev. Biol.* **21**, 350-356.
Bu, W., Chou, A. M., Lim, K. B., Sudhaharan, T. and Ahmed, S. (2009). The Toca-1-N-WASP complex links filopodial formation to endocytosis. *J. Biol. Chem.* **284**, 11622-11636.
Chou, A. M., Sem, K. P., Wright, G. D., Sudhaharan, T. and Ahmed, S. (2014). Dynamin1 is a novel target for IRSp53 protein and works with mammalian enabled (Mena) protein and Eps8 to regulate filopodial dynamics. *J. Biol. Chem.* **289**, 24383-24396.
Croce, A., Cassata, G., Disanza, A., Gagliani, M. C., Tacchetti, C., Malabarba, M. G., Carlier, M.-F., Scita, G., Baumeister, R. and Di Fiore, P. P. (2004). A novel actin barbed-end-capping activity in EPS-8 regulates apical morphogenesis in intestinal cells of Caenorhabditis elegans. *Nat. Cell Biol.* **6**, 1173-1179.
Disanza, A., Mantoani, S., Hertzog, M., Gerboth, S., Frittoli, E., Steffen, A., Berhoerster, K., Kreienkamp, H.-J., Milanesi, F., Di Fiore, P. P. et al. (2006). Regulation of cell shape by Cdc42 is mediated by the synergic actin-bundling activity of the Eps8-IRSp53 complex. *Nat. Cell Biol.* **8**, 1337-1347.
Ellis, S. and Mellor, H. (2000). The novel Rho-family GTPase rif regulates coordinated actin-based membrane rearrangements. *Curr. Biol.* **10**, 1387-1390.
Fan, L. and Mellor, H. (2012). The small Rho GTPase Rif and actin cytoskeletal remodelling. *Biochem. Soc. Trans.* **40**, 268-272.
Goh, L. L. and Manser, E. (2010). The RhoA GEF Syx is a target of Rnd3 and regulated via a Raf1-like ubiquitin-related domain. *PLoS ONE* **5**, e12409.
Goh, W. I., Sudhaharan, T., Lim, K. B., Sem, K. P., Lau, C. L. and Ahmed, S. (2011). Rif-mDia1 interaction is involved in filopodium formation independent of Cdc42 and Rac effectors. *J. Biol. Chem.* **286**, 13681-13694.
Goh, W. I., Lim, K. B., Sudhaharan, T., Sem, K. P., Bu, W., Chou, A. M. and Ahmed, S. (2012). mDia1 and WAVE2 proteins interact directly with IRSp53 in filopodia and are involved in filopodium formation. *J. Biol. Chem.* **287**, 4702-4714.
Govind, S., Kozma, R., Monfries, C., Lim, L. and Ahmed, S. (2001). Cdc42Hs facilitates cytoskeletal reorganization and neurite outgrowth by localizing the 58-kD insulin receptor substrate to filamentous actin. *J. Cell Biol.* **152**, 579-594.
Hall, A. (2012). Rho family GTPases. *Biochem. Soc. Trans.* **40**, 1378-1382.
Kanaji, S., Iwahashi, J., Kida, Y., Sakaguchi, M. and Mihara, K. (2000). Characterization of the signal that directs Tom20 to the mitochondrial outer membrane. *J. Cell Biol.* **151**, 277-288.
Krugmann, S., Jordens, I., Gevaert, K., Driessens, M., Vandekerckhove, J. and Hall, A. (2001). Cdc42 induces filopodia by promoting the formation of an IRSp53:Mena complex. *Curr. Biol.* **11**, 1645-1655.
Lam, C. S., Mistri, T. K., Foo, Y. H., Sudhaharan, T., Gan, H. T., Rodda, D., Lim, L. H., Chou, C., Robson, P., Wohland, T. et al. (2012). DNA-dependent Oct4-Sox2 interaction and diffusion properties characteristic of the pluripotent cell state revealed by fluorescence spectroscopy. *Biochem. J.* **448**, 21-33.
Lim, K. B., Bu, W., Goh, W. I., Koh, E., Ong, S. H., Pawson, T., Sudhaharan, T. and Ahmed, S. (2008). The Cdc42 effector IRSp53 generates filopodia by coupling membrane protrusion with actin dynamics. *J. Biol. Chem.* **283**, 20454-20472.
Linder, S., Wiesner, C. and Himmel, M. (2011). Degrading devices: invadosomes in proteolytic cell invasion. *Annu. Rev. Cell Dev. Biol.* **27**, 185-211.
Manser, E., Huang, H. Y., Loo, T. H., Chen, X. Q., Dong, J. M., Leung, T. and Lim, L. (1997). Expression of constitutively active alpha-PAK reveals effects of the kinase on actin and focal complexes. *Mol. Cell. Biol.* **17**, 1129-1143.
Mattila, P. K., Pykäläinen, A., Saarikangas, J., Paavilainen, V. O., Vihinen, H., Jokitalo, E. and Lappalainen, P. (2007). Missing-in-metastasis and IRSp53 deform PI(4,5)P2-rich membranes by an inverse BAR domain-like mechanism. *J. Cell Biol.* **176**, 953-964.
Pellegrin, S. and Mellor, H. (2005). The Rho family GTPase Rif induces filopodia through mDia2. *Curr. Biol.* **15**, 129-133.
Pykäläinen, A., Boczkowska, M., Zhao, H., Saarikangas, J., Rebowski, G., Jansen, M., Hakanen, J., Koskela, E. V., Peränen, J., Vihinen, H. et al. (2011). Pinkbar is an epithelial-specific BAR domain protein that generates planar membrane structures. *Nat. Struct. Mol. Biol.* **18**, 902-907.
Rigaut, G., Shevchenko, A., Rutz, B., Wilm, M., Mann, M. and Séraphin, B. (1999). A generic protein purification method for protein complex characterization and proteome exploration. *Nat. Biotechnol.* **17**, 1030-1032.
Saarikangas, J., Zhao, H., Pykäläinen, A., Laurinmäki, P., Mattila, P. K., Kinnunen, P. K. J., Butcher, S. J. and Lappalainen, P. (2009). Molecular mechanisms of membrane deformation by I-BAR domain proteins. *Curr. Biol.* **19**, 95-107.
Scita, G., Confalonieri, S., Lappalainen, P. and Suetsugu, S. (2008). IRSp53: crossing the road of membrane and actin dynamics in the formation of membrane protrusions. *Trends Cell Biol.* **18**, 52-60.
Spuul, P., Ciufici, P., Veillat, V., Leclercq, A., Daubon, T., Kramer, I. J. and Génot, E. (2014). Importance of RhoGTPases in formation, characteristics, and functions of invadosomes. *Small GTPases* **5**, e28195.
Suetsugu, S., Kurisu, S., Oikawa, T., Yamazaki, D., Oda, A. and Takenawa, T. (2006). Optimization of WAVE2 complex-induced actin polymerization by membrane-bound IRSp53, PIP(3), and Rac. *J. Cell Biol.* **173**, 571-585.
Vingadassalom, D., Kazlauskas, A., Skehan, B., Cheng, H.-C., Magoun, L., Robbins, D., Rosen, M. K., Saksela, K. and Leong, J. M. (2009). Insulin receptor tyrosine kinase substrate links the *E. coli* O157:H7 actin assembly effectors Tir and EspF(U) during pedestal formation. *Proc. Natl. Acad. Sci. USA* **106**, 6754-6759.
Weiss, S. M., Ladwein, M., Schmidt, D., Ehinger, J., Lommel, S., Städing, K., Beutling, U., Disanza, A., Frank, R., Jansch, L. et al. (2009). IRSp53 links the enterohemorrhagic *E. coli* effectors Tir and EspFU for actin pedestal formation. *Cell Host Microbe* **5**, 244-258.
Zhao, H., Pykäläinen, A. and Lappalainen, P. (2011). I-BAR domain proteins: linking actin and plasma membrane dynamics. *Curr. Opin Cell Biol.* **23**, 14-21.
Zwaenepoel, I., Naba, A., Da Cunha, M. M. L., Del Maestro, L., Formstecher, E., Louvard, D. and Arpin, M. (2012). Ezrin regulates microvillus morphogenesis by promoting distinct activities of Eps8 proteins. *Mol. Biol. Cell* **23**, 1080-1095.